Climate controls the length and shape of the world's drainage basins

Michael Bliss Singer[1,2,3*], Stuart W.D. Grieve[4], Shiuan-An Chen[5], Katerina Michaelides[3,5]

[1]School of Earth and Ocean Sciences, Cardiff University, Main Building, Park Place, Cardiff, CF10 3AT, UK.

[2]Water Research Institute, Cardiff University, The Sir Martin Evans Building, Museum Avenue, Cardiff, CF10 3AX, UK.

[3]Earth Research Institute, University of California Santa Barbara, Ellison Hall, Santa Barbara, CA 91306, USA.

[4]School of Geography, Queen Mary University of London, London, E1 4NS, UK.

[5]School of Geographical Sciences, University of Bristol, Bristol, BS8 1SS, UK.

[*]**Email:** bliss@eri.ucsb.edu.

Abstract

Climate is thought to affect the structure and evolution of drainage basins, yet it is still widely held that there is universal power law scaling between channel length and drainage area, which is independent of climate. Since climate controls runoff, streamflow, and erosion regimes, we looked for climate dependency within a new, global dataset of drainage basin morphometrics. We show that increasingly arid drainage basins have longer channels and narrower drainage basins, and power law scaling increases monotonically with aridity. We suggest these results arise due to downstream channel extension by extreme events, wherein increasingly large floods erode channels into previously unchanneled terrain, yielding a morphometric signature in drylands that is preserved over long timescales due to a lack of biotic smoothing of topography. This new understanding of drainage basin morphometrics on Earth may be used to inform interpretations of past climates on Earth and other solar system bodies.

1. Introduction

Metrics of topography and topology from drainage networks provide information about the forces involved in their formation (Chen et al., 2019; Dunne, 1990; Horton, 1945; Perron et al., 2012; Rinaldo et al., 1995; Seybold et al., 2017; Slater & Singer, 2013). Channel length (*L*) is a metric describing the topographic expression of along-channel distance from source to mouth (*Supporting Information*). Length is fundamentally affected by channel head position (the point in

the landscape at which fluvial erosion exceeds sediment input (Montgomery & Dietrich, 1988)) and the downstream limits on topographic channel extension. Channel head position is assumed to be approximately fixed for a given stationary climate regime, for example, where larger upstream drainage areas are required to incise a channel head in more arid climates due limits on the production of water (Montgomery & Dietrich, 1988). The downstream extent of channels is controlled by the presence of downstream water bodies. For example, perennial river channels in humid regions typically debouch into a higher order stream, lake, sea, or ocean, while endorheic (internally draining) basins, common to drylands, are only limited in their downstream extent by the supply of water from upstream required to erode the channel farther downstream. Drainage basin area (*A*), or area upstream of the most downstream point on a channel, reflects the topological spreading of the channel network, bifurcation frequency, and tributary junction angles (Horton, 1945; Montgomery & Dietrich, 1988; Seybold et al., 2017; Yi et al., 2018), and the along-channel length to area ratio (*L*/*A*) expresses how much the dominant channel fills its drainage area. *L*/*A* can be thought of as a hydrologic aspect ratio, and it is an approximate measure of basin shape. Higher values of *L/A* correspond to relatively short channels in wider basins and lower values represent relatively long channels in narrow basins.

The relationship between *L* and *A* is generalized regionally and across the globe by Hack's Law *(L* $= \underline{\underline{c}}A^h$), where *c* is a dimensionless coefficient and *h* is a dimensionless exponent. This empirical formulation is based on regional field surveys (Hack, 1957), which was later shown to emerge statistically based on fractal characteristics in natural networks (Rigon et al., 1996). The Hack's Law exponent *h* has been shown to be approximately 0.6 from datasets, theoretical analysis, and lab experiments (Rigon et al., 1996). Hack's Law is a widely agreed upon universal, increasing relationship between channel length and drainage area for the world's basins (Hack, 1957), which is commonly used to characterize the emergent properties of networks on Earth and other planetary bodies (Rigon et al., 1996), to quantify hydrologic response times (Rinaldo et al., 1998), and to parameterize geomorphic landscape evolution models in order to assess the effects of tectonics and other environmental phenomena on network development (Tucker & Whipple, 2002).

Each of these diagnostic drainage basin morphometrics (*L*, *A*, *L*/*A, h*) should vary across the globe, depending on the regionally relevant set of controls (climate, lithology, tectonics, land use). Generalizations of drainage basin evolution have largely focused on time as the key variable, arguing that networks become more elaborate over longer timescales following tectonic uplift or base level change, and that they may develop in random fashion (Leopold et al., 1964; Rinaldo et

al., 1998). Implicit in these generalizations is an assumption that climatic forcing is more equivocal in terms of its systematic imprint within morphometrics. However, climate controls the regional water cycle and its translation into streamflow generation, channel erosion regimes, and vegetative resistance, so its expression over the relevant spatial and temporal scales must have a primary influence on drainage network development (Chen et al., 2019; Collins & Bras, 2008; Tucker, 2004). Since climate is nonuniformly expressed across the globe, we might expect to see broad differences in drainage basin metrics in distinct climatic zones, irrespective of spatial variations in lithology, tectonics, and land use.

Recent research has indicated that regional climate controls some aspects of drainage network topography and topology (Bonnet, 2009; Chen et al., 2019; Rinaldo et al., 1995; Seybold et al., 2017; Slater & Singer, 2013; Solyom & Tucker, 2004; Tucker & Bras, 2000; Yi et al., 2018). Some of these studies suggest that arid climate zones have a higher number of narrower drainage basins for a given area than humid climate zones and that the drainage area upstream of a channel head is larger for arid regions. However, it is challenging to generalize the understanding of climatic controls on drainage basins from previous research beyond the local site/region of study, dataset, model setup, or laboratory flume conditions.

2. Methods

To investigate the influence of climate on drainage basin morphometrics over a wide range of climates, we developed a new, open-access Global Drainage Basin Morphometrics database (GDBM) between 60°N and 56°S (Fig.S1a;Dataset S1). The creation of a new database was required to explore morphometrics in basins that exist entirely within a single climate regime, to investigate channel topography instead of river hydrography, and in order to characterize how morphometrics vary across a spectrum of humid and arid climate zones, the latter of which are less studied (*Supporting Information*).

This near-global, spatially explicit drainage basin dataset was extracted from NASA's 30-m Shuttle Radar Topography Mission Digital Elevation Model (SRTM-DEM), using software designed for extracting morphometrics with speed and reproducibility, and without prior assumptions about channel locations or extent (*Supporting Information*). The GDBM database enables: 1) analysis of key basin morphometrics (*L*, *A, L/A*) from all basins above a consistent threshold area (*Supporting Information*); 2) characterization of Hack's *h*, the scaling between channel length and drainage area, for a range of *A* over which Hack's *h* is not expected to vary (Willemin, 2000); and 3) quantification of the number of drainage basins or subbasins within particular regions or climate

categories. Subbasins refer to subdivisions of a basin that contains more than one extracted channel that exceeds the drainage area threshold (*Supporting Information*).

We interrogated GDBM to generalize about the role of climate in drainage basin evolution using the Köppen-Geiger climate classification (Fig.S1b) and categories of the quantitative Aridity Index (Precipitation/Potential Evapotranspiration, Fig.S1c). Köppen-Geiger incorporates various rules regarding temperature and precipitation thresholds emphasizing vegetation response to climate. Aridity Index, a scale that (nonintuitively) declines with aridity, more straightforwardly characterizes the hydrologic expression of climate as a simplified water balance. We use these classifications to test whether aridity in the hydrologic cycle is detectable in key basin morphometrics. By climate-classifying the basins, and also by limiting our analysis to small basins (*Supporting Information*), we can more straightforwardly constrain and explore the climatic controls on drainage basins development. We treat the two classifications independently in our analysis and pose the null hypothesis that there are no differences in morphometrics between climate categories in each. To simplify the analysis, we did not control for other natural or anthropogenic variables, which likely produce higher variability in the resulting data. Therefore, we posit that any signals that arise from these environmental data based on climatic classifications can be assumed to be strong enough to overprint the scattering effects of other variables.

3. Results

In total, we documented 355,123 individual drainage basins within GDBM, including mainstem channels and subbasin channels that exceed the threshold area (*Supporting Information*). Of this total number of drainage basins, our analysis of climate dependency in morphometrics includes only those entirely contained within one Köppen-Geiger climate subzone (72% of extracted channels), and it excludes those spanning two or more Köppen-Geiger subzones (28%) (Fig.S2; Table S1). Global medians of L, A, and L/A for channels contained within a single Köppen-Geiger climatic subzone are 32 km, 220 km^2, and 0.14 km/km^2, respectively (Fig.1, Figs.S4;S5).

But are climatic signatures systematically expressed within drainage basin metrics globally? L is similar among the four main Köppen-Geiger categories except the Arid category, which contains relatively long channels with high values of L/A (Fig.1a,c). Looking at the role of aridity in more detail, we found that surprisingly, within the Aridity Index classification, L and L/A increase systematically with increasing aridity (Fig.1b,d). Furthermore, if we group the GDBM basins into dryland (Semi-arid, Arid, Hyperarid) versus non-dryland (Dry Subhumid, Humid) categories, we

140 find that dryland channels are disproportionately longer with higher values of *L/A*. This result
141 holds despite no systematic differences in drainage basin areas between classes, apart from
142 notably larger basins in the Hyperarid Aridity Index category (Fig.1e-f; Fig.S4d-f).
143
144 These findings suggest a systematic control of climate on drainage basin development in
145 drylands, in which higher aridity produces progressively longer channels and narrower drainage
146 basins. The results are consistent with prior observations suggesting that arid regions produce
147 narrower drainage basins (Bonnet, 2009) with more acute junction angles (Seybold et al., 2017),
148 yet it contrasts with previous research indicating that arid regions have shorter channels for a
149 given drainage area (Yi et al., 2018). It also contradicts prior work suggesting that Hack's *h* is not
150 sensitive to climate (Sassolas-Serrayet et al., 2018).
151
152 To investigate this further, we looked for climate dependency within Hack's Law. It is generally
153 assumed that Hack's Law provides a universal scaling relationship between *L* and *A* for channels
154 across the globe, and that Hack's *h* only varies with basin area (Rigon et al., 1996; Willemin, 2000)
155 above a threshold of ~20,000 km^2 (well above the scale of basins studies here, *Supporting*
156 *Information*), and not with basin shape (Sassolas-Serrayet et al., 2018). We plotted the *L* versus *A*
157 data from GDBM classified by Aridity Index on a log-log scale and computed *h* based on least
158 squares regression for each Aridity Index category (Fig.2).
159
160 Surprisingly, we found that the global average value of *h* (0.758) for all basins is ~25% higher than
161 what has been reported (Hack, 1957; Rigon et al., 1996), suggesting that channels are longer for a
162 given basin area than previously thought. Upon further investigation, we found that this
163 difference can be explained by the method of computing channel length. Specifically, our method
164 accounts for sinuosity along the channel, which we feel most accurately represents channel
165 length and consequently, fluvial processes, while previous work has apparently relied on simple
166 Euclidean distance along the channel axis or utilized coarser data (*Supporting Information*;Fig.S3).
167
168 Regarding climate dependence, we found an unprecedented result that *h* systematically
169 increases with aridity (from 0.746 to 0.796 between Humid and Hyperarid basins, respectively,
170 Fig.2). This result is corroborated by the fact that the Arid zone within the Köppen-Geiger
171 classification also has the highest value of *h* (Fig.S6).
172
173 A recent paper obtained the opposite result, namely that Hack's *h* is systematically lower for arid
174 basins than humid ones within the continental USA (Yi et al., 2018). However, that study used a

hydrography dataset developed by a drainage enforcement technique that involves burning previously mapped stream networks (blue lines) into a digital elevation model. Our results are not directly comparable to that study because drainage enforcement would always yield shorter river lengths for dryland regions, as arid channels flow discontinuously and less frequently and therefore their full extent does not show up on stream network maps (*Supporting Information*). In contrast, our unsupervised approach to channel extraction identifies the full extent of channels within humid and arid areas alike (subject the limits of the 30-m SRTM dataset), revealing a strong climate dependency in Hack's *h* (Fig.2; Fig.S6).

Another recent study showed that Hack's *h* is insensitive to climate (mean annual rainfall, rather than aridity) and shape (Sassolas-Serrayet et al., 2018), but that study focused on one of the most tectonically active areas of the world (Himalayas), where tectonic forcing would tend to overprint any climatic controls on drainage basin development (Tucker, 2004). That study argued that the Hack's Law dimensionless coefficient, *c*, is a more sensitive parameter that reflects basin shape. Correspondingly, in corroboration of the Hack's *h* results, we also found from GDBM that Hack's *c* monotonically increases with aridity (*Supporting Information*), further supporting the conclusion that basin shape becomes more elongate (Sassolas-Serrayet et al., 2018) in drier climatic regions.

4. Discussion

We view the *L*, *L/A* , and Hack's *h* results (Fig.1) as global confirmation of the tendency for longer, narrow drainage basins to develop in arid climates typified by precipitation/runoff regimes that are highly variable in space and time (Bonnet, 2009; Seybold et al., 2017; Solyom & Tucker, 2004; Tucker & Bras, 2000), but by what potential mechanisms? It has been suggested that arid regions have relatively high areas of unchannelized basin due to limited runoff generation at small drainage areas (Montgomery & Dietrich, 1988), so we expected to find correspondingly short arid channel lengths. In fact, the GDBM pattern is the opposite, namely higher *L* and *L/A* in progressively more arid environments (Fig.1b,d;Figs.S4;S5). These results are strong evidence of a climatic control on drainage basin evolution favoring network extension (channel elongation) (Wolman & Gerson, 1978) and splitting of drainages into narrow basins in arid regions (Bonnet, 2009).

Given the obvious limitation of water in arid regions, what might explain longer channels and higher values of *L/A*? Dryland hydrology is characterized by brief spells of often intense rainfall expressed over a limited area of a basin, partial area runoff during intense rainstorms, and the development of channel flow only when the period of runoff generation is long enough (Carson &

Kirkby, 1972; Michaelides et al., 2018b; Singer & Michaelides, 2017). Dryland channel flow regimes are characterized by long periods of no flow, discontinuous flow along the channel, and infrequent extreme flood events that topographically reshape channels due to inherently low erosion thresholds (Singer & Michaelides, 2014; Wolman & Gerson, 1978). Channel bed erosion can occur easily in drylands, in part due to a lack of vertical sorting and channel bed armoring associated with high sediment supply during brief flood events that is incompletely sorted along the channel (Laronne et al., 1994; Singer & Michaelides, 2014). Arid basins also tend to be internally draining (endorheic), so they typically do not have a base level that is fixed by a perennial water body (larger river, lake, or sea), as is often the case in humid environments. Thus, arid channels have room to grow downstream, with a measurable topographic imprint, when the conditions are suitable.

These factors enable channel elongation by downstream extension of the arid fluvial network during rare, extreme flood events (Leopold & Miller, 1962; Rinaldo et al., 1995; Wolman & Gerson, 1978). Upstream extension of the network in drylands is unlikely due to limits on the generation of runoff capable of eroding a channel head (Montgomery & Dietrich, 1988). The topographic imprint of downstream channel extension arising from infrequent extreme events may be subsequently preserved over long timescales (Solyom & Tucker, 2004; Tucker & Bras, 2000), due to the limited effects of vegetation and bioturbation in arid regions (Rinaldo et al., 1995; Wolman & Gerson, 1978). Furthermore, arid basins tend to have limited sediment delivery from upstream that might otherwise infill the channel and obscure the signature of episodic erosion because flood events derived from dryland rainstorms are too short-lived and spatially restricted to efficiently export sediment from upstream to downstream (Michaelides et al., 2018a; Singer & Michaelides, 2014; Singer & Michaelides, 2017). Thus, we observe longer channels, higher *L/A*, and higher Hack's *h* in progressively arid regions (Figs.1;2).

The general differences between humid and arid regions in terms of drainage basin morphology are summarized schematically (Fig.3a-b) and correspondingly for extracted basins in GDBM (Fig.3c-d), while Fig.3e shows how the key morphometrics studied here vary with aridity. In summary, our analysis revealed clear climatic signatures within drainage basin morphometrics across the globe without controlling for additional interacting independent variables such as tectonics or land use. These climate signatures can be seen in both Köppen-Geiger and Aridity Index classifications.

We showed that *L*, *L/A*, and Hack's *h* increase with aridity, while *A* is mostly insensitive to climate (Figs.1b,d-f;2;3e;Figs.S4;S5). This suggests that aridity in basins preserves major erosion episodes and their downstream extension of drainage networks, producing long, narrow basins that are closely spaced (Bonnet, 2009; Perron et al., 2009), and that preservation of the imprint of these extreme events is higher with increasing aridity (*sensu* (Rinaldo et al., 1995)). Finally, we found that the number of classified drainage basins in GDBM (< 3000 km^2, Fig.S4) increases from Hyperarid to Semi-arid aridity classes, then drops again in the Dry Subhumid class, before reaching its maximum in the Humid class (n=114,201;Fig.3e;Table S1). This latter result may indicate a bimodality in drainage basin organization due to feedbacks between climate and vegetation. It suggests that many narrow subbasins are created in Semi-arid environments via network splitting (Bonnet, 2009), yielding higher sediment loads where there is enough water to erode the landscape by overland flow (Horton, 1945), but where there is not enough vegetation to resist this erosion (Collins & Bras, 2008). Once the vegetation becomes more dense in Dry Subhumid basins, the water travels along subsurface flow paths (Dunne, 1990), leading to topological spreading that increases drainage density (Collins & Bras, 2010) and generates numerous subbasins in Humid basins (Fig.3).

The morphometric patterns observed here lend strong support to the hypothesis that climate plays a first-order role in drainage basin development, broadly supporting evidence from previous research (Bonnet, 2009; Chen et al., 2019; Seybold et al., 2017; Solyom & Tucker, 2004). While there are numerous published examples of how drainage basin evolution is influenced by independent variables such as human impacts, tectonics, and lithology, we show that climate leaves indelible signatures within morphometrics. These signatures are clearly detectable, irrespective of multiple confounding factors and regardless of the climate classification scheme used. They may provide insights into how drainage basins will evolve to climate change on Earth and into the climate history of other solar system bodies.

References

Bonnet, S. (2009). Shrinking and splitting of drainage basins in orogenic landscapes from the migration of the main drainage divide. *Nature Geosci, 2*(11), 766-771. 10.1038/ngeo666. http://dx.doi.org/10.1038/ngeo666

Carson, M. A., & Kirkby, M. J. (1972). *Hillslope Form and Process*: Cambridge University Press.

Chen, S.-A., Michaelides, K., Grieve, S. W. D., & Singer, M. B. (2019). Aridity is expressed in river topography globally. *Nature, 573*, 573–577. https://doi.org/10.1038/s41586-019-1558-8

Collins, D. B. G., & Bras, R. L. (2008). Climatic control of sediment yield in dry lands following climate and land cover change. *Water Resources Research, 44*(10), 8. Article. <Go to ISI>://000259993200002

Collins, D. B. G., & Bras, R. L. (2010). Climatic and ecological controls of equilibrium drainage density, relief, and channel concavity in dry lands. *Water Resources Research, 46*(4), W04508. http://dx.doi.org/10.1029/2009WR008615

Dunne, T. (1990). Hydrology, mechanics, and geomorphic implications of erosion by subsurface flows. In C. G. Higgins & D. R. Coates (Eds.), *Groundwater geomorphology: The role of subsurface water in earth-surface processes and landforms* (pp. 1-28). Boulder, CO: Geol. Soc. Amer. Special Paper 252.

Hack, J. T. (1957). *Studies of longitudinal stream profiles in Virginia and Maryland* (294-B). Retrieved from Menlo Park, CA:

Horton, R. E. (1945). Erosional development of streams and their drainage basins; hydrophysical approach to quantitative geomorphology. *Geol. Soc. Amer. Bull., 56*, 275-370.

Laronne, J. B., Reid, I., Yitshak, Y., & Frostick, L. E. (1994). The non-layering of gravel streambeds under ephemeral flood regimes. *Journal of Hydrology, 159*(1-4), 353-363. http://www.sciencedirect.com/science/article/B6V6C-487DTBV-16/2/208964486e0bc7aaa3836d7dad610ccb

Leopold, L., Wolman, M. G., & Miller, J. P. (1964). *Fluvial Processes in Geomorphology*. San Francisco, CA: W.H. Freeman & Co.

Leopold, L. B., & Miller, J. (1962). *Ephemeral streams: hydraulic factors and their relation to the drainage net*. Retrieved from Washington, D.C.:

Michaelides, K., Hollings, R., Singer, M. B., Nichols, M. H., & Nearing, M. A. (2018a). Spatial and temporal analysis of hillslope–channel coupling and implications for the longitudinal profile in a dryland basin. *Earth Surface Processes and Landforms*. http://dx.doi.org/10.1002/esp.4340

Michaelides, K., Hollings, R., Singer, M. B., Nichols, M. H., & Nearing, M. A. (2018b). Spatial and temporal analysis of hillslope–channel coupling and implications for the longitudinal profile in a dryland basin. *43*(8), 1608-1621. https://onlinelibrary.wiley.com/doi/abs/10.1002/esp.4340

Montgomery, D. R., & Dietrich, W. E. (1988). Where do channels begin. *Nature, 336*(6196), 232-234. <Go to ISI>://WOS:A1988Q954200042

Perron, J. T., Kirchner, J. W., & Dietrich, W. E. (2009). Formation of evenly spaced ridges and valleys. *Nature, 460*(7254), 502-505. <Go to ISI>://WOS:000268257000036

Perron, J. T., Richardson, P. W., Ferrier, K. L., & Lapotre, M. (2012). The root of branching river networks. *Nature, 492*(7427), 100-103. 10.1038/nature11672. http://dx.doi.org/10.1038/nature11672

Rigon, R., Rodriguez-Iturbe, I., Maritan, A., Giacometti, A., Tarboton, D. G., & Rinaldo, A. (1996). On Hack's Law. *32*(11), 3367-3374. https://agupubs.onlinelibrary.wiley.com/doi/abs/10.1029/96WR02397

Rinaldo, A., Dietrich, W. E., Rigon, R., Vogel, G. K., & Rodrlguez-lturbe, I. (1995). Geomorphological signatures of varying climate. *Nature, 374*(6523), 632-635. 10.1038/374632a0. http://dx.doi.org/10.1038/374632a0

Rinaldo, A., Rodriguez-Iturbe, I., & Rigon, R. (1998). Channel networks. *Annual Review of Earth and Planetary Sciences, 26*(1), 289-327. https://www.annualreviews.org/doi/abs/10.1146/annurev.earth.26.1.289

Sassolas-Serrayet, T., Cattin, R., & Ferry, M. (2018). The shape of watersheds. *Nature Communications, 9*(1), 3791. https://doi.org/10.1038/s41467-018-06210-4

Seybold, H., Rothman, D. H., & Kirchner, J. W. (2017). Climate's watermark in the geometry of stream networks. *Geophysical Research Letters, 44*(5), 2272-2280. http://dx.doi.org/10.1002/2016GL072089

Singer, M. B., & Michaelides, K. (2014). How is topographic simplicity maintained in ephemeral dryland channels? *Geology, 42*(12), 1091-1094. http://geology.gsapubs.org/content/42/12/1091.abstract

Singer, M. B., & Michaelides, K. (2017). Deciphering the expression of climate change within the Lower Colorado River basin by stochastic simulation of convective rainfall. *Environmental Research Letters, 12*.

Slater, L. J., & Singer, M. B. (2013). Imprint of climate and climate change in alluvial riverbeds: Continental United States, 1950-2011. *Geology, 41*(5), 595-598. http://geology.gsapubs.org/content/41/5/595.abstract

Solyom, P. B., & Tucker, G. E. (2004). Effect of limited storm duration on landscape evolution, drainage basin geometry, and hydrograph shapes. *Journal of Geophysical Research-Earth Surface, 109*(F3). <Go to ISI>://000236711300001

Tucker, G. E. (2004). Drainage basin sensitivity to tectonic and climatic forcing: Implications of a stochastic model for the role of entrainment and erosion thresholds. *Earth Surface Processes and Landforms, 29*(2), 185-205. <Go to ISI>://000189226700005

Tucker, G. E., & Bras, R. L. (2000). A stochastic approach to modeling the role of rainfall variability in drainage basin evolution. *Water Resources Research, 36*(7), 1953-1964. <Go to ISI>://000087928800028

Tucker, G. E., & Whipple, K. X. (2002). Topographic outcomes predicted by stream erosion models: Sensitivity analysis and intermodel comparison. *J. Geophys. Res., 107*(B9), 2179. http://dx.doi.org/10.1029/2001JB000162

Willemin, J. H. (2000). Hack's Law: Sinuosity, convexity, elongation. *Water Resources Research, 36*(11), 3365-3374. https://agupubs.onlinelibrary.wiley.com/doi/abs/10.1029/2000WR900229

Wolman, M. G., & Gerson, R. (1978). Relative time scales of time and effectiveness of climate in watershed geomorphology. *Earth Surface Processes & Landforms, 3*, 189-208.

Yi, R. S., Arredondo, Á., Stansifer, E., Seybold, H., & Rothman, D. H. (2018). Shapes of river networks. *Proceedings of the Royal Society A: Mathematical, Physical and Engineering Sciences, 474*(2215), 20180081.

Acknowledgments

General: This research utilized Queen Mary's Apocrita HPC facility, supported by QMUL Research-IT. http://doi.org/10.5281/zenodo.438045. **Funding**: This work was partially supported by NSF (BCS-1660490 and EAR-1700555 to M.B.S), SERDP (RC18-1006 to M.B.S.), and NERC (NE/P015786/1 to K.M.). **Author Contributions**: M.B.S. and K.M. conceived of the research. M.B.S., S.W.D.G., and S-A.C. performed the analysis. M.B.S. and S-A.C. generated the figures. M.B.S., K.M., and S.W.D.G. contributed to interpretation of data. M.B.S. wrote the paper. K.M. and S.W.D.G. provided edits to the manuscript. **Competing Interests**: None declared. **Data and Material Availability**: All data in the manuscript are available in the supplementary materials or at: https://ucsb.box.com/s/fep0g3nayxq6k290v2z422yypvju1ubg.

Figures

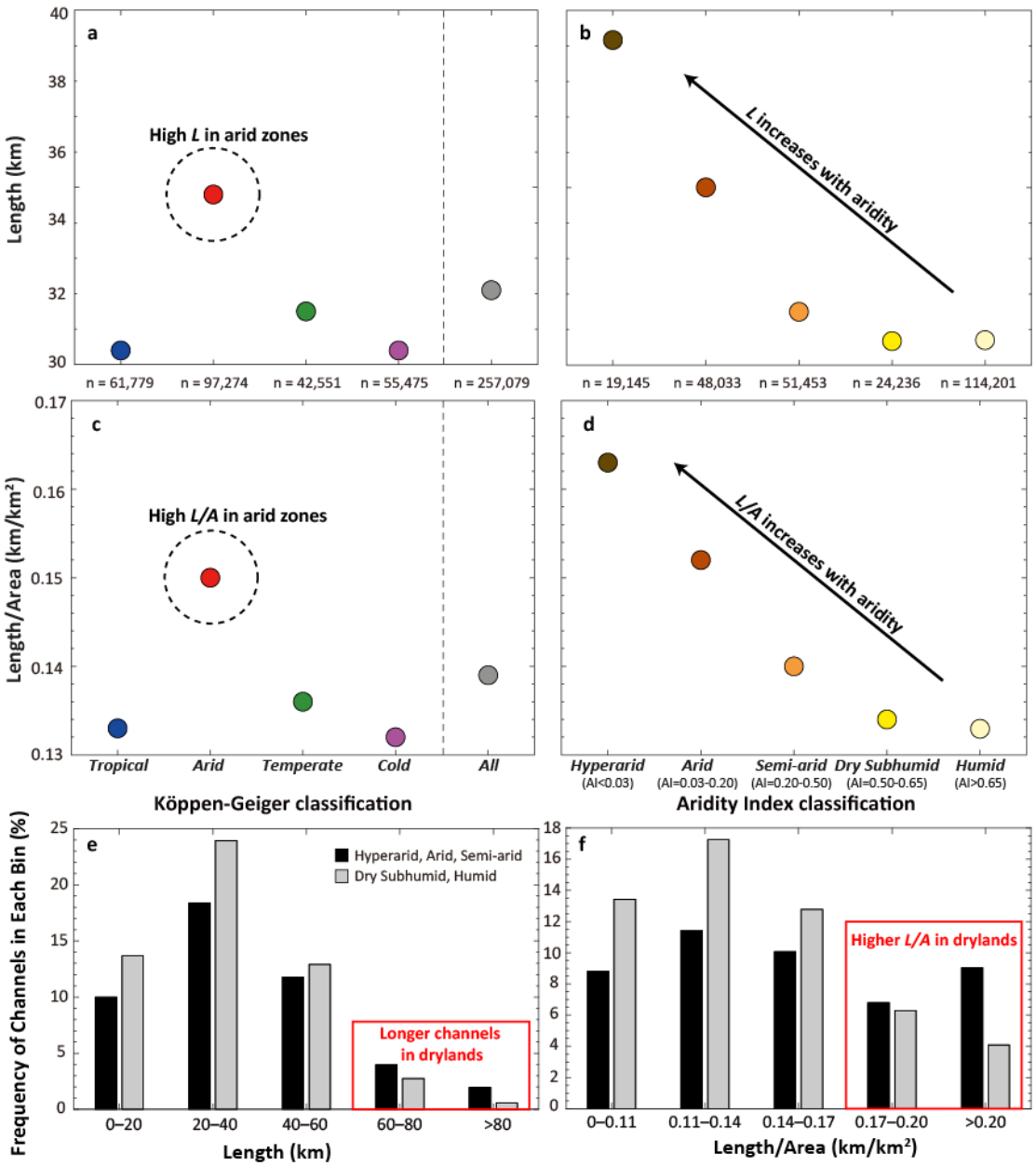

Fig. 1 | Morphometrics from GDBM for Köppen-Geiger and Aridity Index climate classifications. Median values of distributions by main Köppen-Geiger zone and Aridity Index classes for channel length, *L* (**a,b**) and *L/A* (**c,d**), corresponding to the distributions in Figs.S4;S5. Number of basins in each climate category is contained below **a** and **b**. Panels **e** and **f** shows the frequency (%) of basins by bins of *L* (**e**) and *L/A* (**f**), grouped by drylands (Hyperarid, Arid, Semi-arid) versus non-drylands (Dry Subhumid, Humid) from the Aridity Index classification.

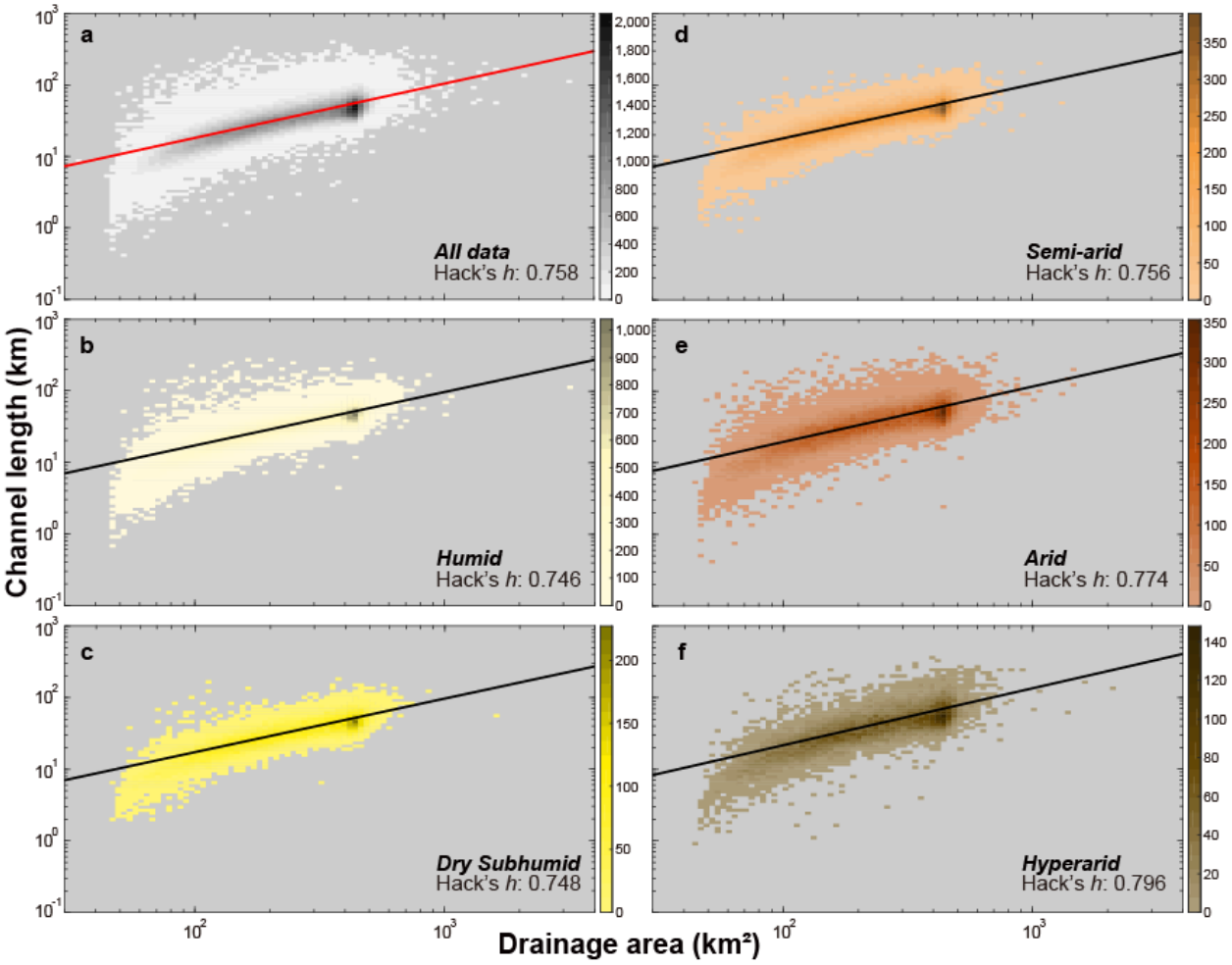

Fig. 2 | Climate-classified Hack's Law. Data by Aridity Index category for relationships between channel length (*L*) and drainage area (*A*). Density of points in areas of the scatterplot are shown in the scale bars to the right of each panel. All data are shown in panel **a**. The Hack exponents (*h*) for each panel (**b-f**) indicate a climatic dependency on the steepness of this relationship, where increasing aridity yields a higher value of *h*.

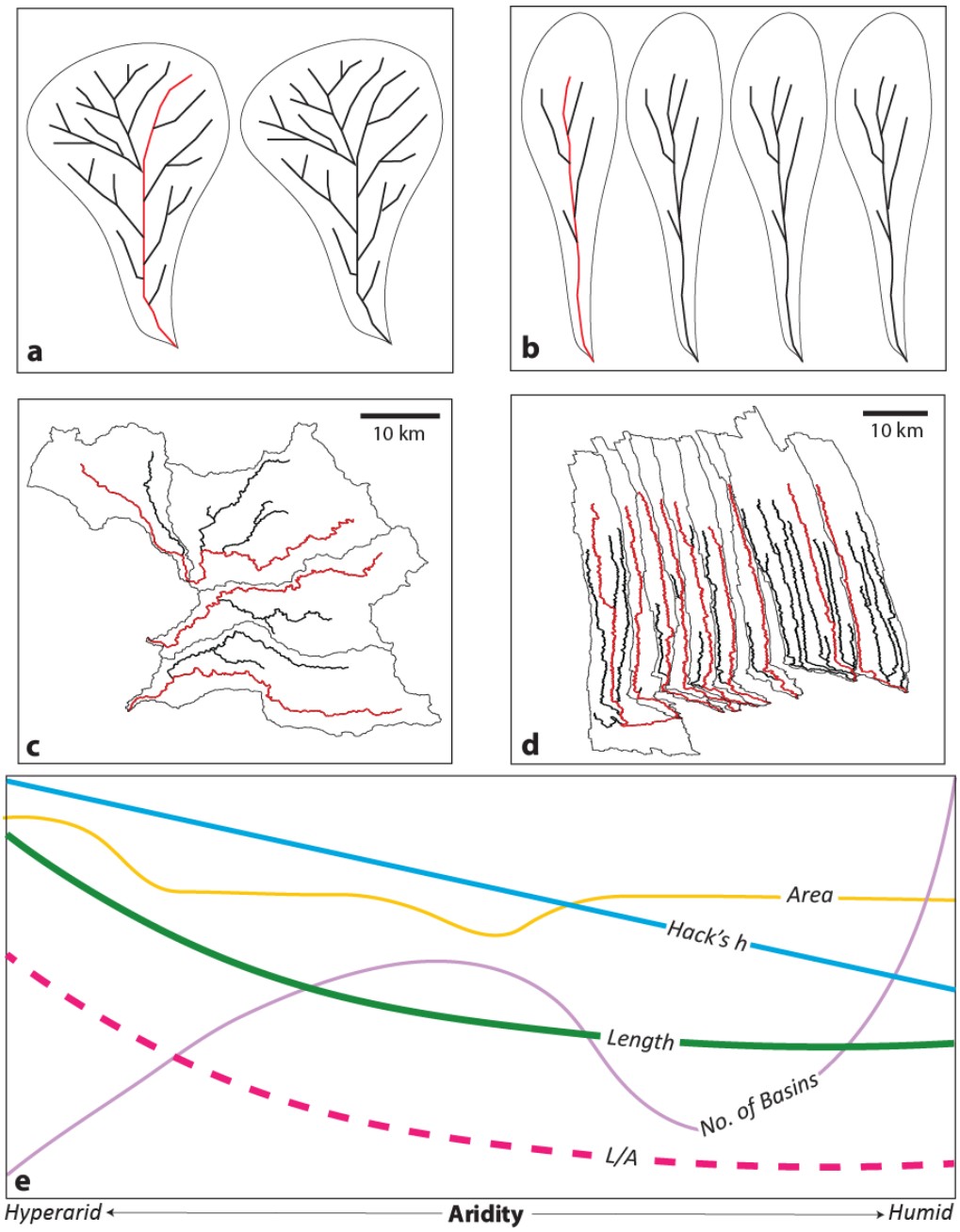

Fig. 3 | Climatic controls on drainage basins. Schematic of drainage basin size and length within a spatial area of humid (**a**) and arid (**b**) basins. Red trace on each plot indicates the longest (highest order) channel (mainstem). Example drainage basins of similar basin area extracted from SRTM-DEM for humid (**c**) and arid (**d**) climates in the Philippines and Australia (the area in each box corresponds to 2900 and 4000 km^2, respectively). Panel **e** summarizes how channel length, drainage area, *L/A*, Hack's *h*, and number of basins vary with aridity.

Supporting Information for 'Climate controls the length and shape of the world's drainage basins' by Singer et al.

Rationale for a New Global Database. Our aim in this study was to investigate drainage basin morphometrics stratified by climatic forcing across the globe without making any assumptions about hydrography from previously created maps. We sought to investigate morphometrics and their climatic dependence in an unbiased way, and at a scale appropriate for identifying climatic controls on drainage basin developments. Although global hydrography datasets exist, e.g., (Lehner et al., 2008; Ouellet Dallaire et al., 2019), none contained the relevant information to accomplish these goals. In particular, we required accurate topographic metrics (Grieve et al., 2016) within individual small drainage basins and their subbasins that lie entirely within a single climatic zone, so we could isolate the effects of climate on drainage basin development. Additionally, we needed morphometrics from all channels within drainage basins that have topographic expression, irrespective of whether they contain water and would be mapped as blue lines on topographic maps. Widely used global river hydrography datasets (e.g., HydroSHEDS (Lehner et al., 2008)) and corresponding classifications based upon them (e.g., GLoRiC (Ouellet Dallaire et al., 2019)) were developed using ~90 m (3 arc second) SRTM data, so they are not appropriate for analysis of small basins. Furthermore, they are focused on perennial rivers, relying on drainage enforcement (or stream burning) techniques to confirm channel locations, so they cannot be used to explore how drainage basin morphometrics vary across a wide range of climates including arid regions where blue lines are typically not mapped for ephemeral channels because they are not readily visible and are therefore not stored in hydrography GIS layers. This may lead to analysis biases toward humid regions and errors of interpretation for arid region. We have shown in previous work (Chen et al., 2019), that interesting lessons can be learned from fully investigating drainage basin topographic morphometrics across climatic gradients from Humid to Hyperarid.

To fill this gap, we developed a new global database of drainage basin morphometrics (GDBM), which relies on the same underlying DEM (SRTM) used as the basis for most other global river databases. However, three major differences between GDBM and existing databases are: 1) our database is built upon the higher resolution SRTM DEM (1 arc second or 30-m at the equator); 2) our channel extraction methods include all channels above a drainage area threshold, whether dry or wet; and 3) we limit our analysis to drainage basins in which the longest channel does not cross Köppen-Geiger climate zone boundaries (see below for details).

Creation of Global Drainage Basin Morphometrics (GDBM). In order to create the GDBM database (Fig.S1a), the 30-m global Shuttle Radar Topography Mission (SRTM) DEM was broken into contiguous climate zone tiles based on Köppen-Geiger climate subzone data (Fig.S1b; (Peel et al., 2007)). This allowed each individual climate zone segment to be processed in parallel. In some cases, the Köppen-Geiger climate subzones were still too large to be efficiently processed and were further subdivided. The result of this processing was a collection of 1,805 DEM tiles (Fig.S2a), each corresponding to a single contiguous Köppen-Geiger climate subzone.

Fluvial networks were extracted for each of these DEM tiles using LSDTopoTools (Clubb et al., 2017). The DEM tile was first hydrologically corrected, using an algorithm which removes local topographic depressions (sinks) from the data, allowing each pixel in the tile to flow to the local base level (Wang & Liu, 2006). The initiation point of each channel was identified using an area-threshold technique (Tarboton David et al., 1991), which identifies each cell in the DEM which exceeds the threshold drainage area and has no upslope cells of higher drainage area (Fig.S2). We did not correct for any local effects (e.g., vegetation cover) because we did not want to introduce any user artifacts into the dataset that would limit the power of the internally consistent 30-m SRTM DEM. We worked under the assumption that the roughness of vegetation along channels responds directly to the underlying topography, so we can detect channel morphometrics, even under vegetation cover. Most importantly, we sought to have a product that required the minimum amount of processing prior to channel extraction.

The accuracy of any channel extraction methodology is governed in part by the resolution of the topographic data being used. It has been demonstrated that attempting to identify channel initiation points using non-threshold based methods in 30-m resolution data is challenging, particularly in the headwaters of catchments, where signals of fluvial incision are less pronounced and more transient (Montgomery & Dietrich, 1988). These challenges are even more pronounced in the case of a global analysis, where an area threshold appropriate for one landscape will be unsuitable for another. As channel extraction confidence is proportional to channel size (Grieve et al., 2016), a deliberately conservative drainage area threshold of 22.5 km^2 was employed for this study, irrespective of latitude. This value balances the need for computational efficiency with the requirement to extract the properties of the longest subbasin channel in which we can have confidence. Note that we did not extract any channels from the Polar zone of the Köppen-Geiger classification in order to avoid permanent snow/glacier coverage that would obscure channel topography.

From the extracted channel initiation points, steepest descent traces were run downslope until every initiation point connected with the lowest point in each tile. The steepest descent algorithm used is the D8 method, which directs flow based on the gradient between the DEM cell of interest and its 8 neighboring cells (Fig.S2). This procedure is optimized as described by the FastScape algorithm (Braun & Willett, 2013), to allow it to be run on such a large dataset. These channels were further processed to ensure that only channels entirely contained within a tile (Köppen-Geiger climate subzone) were sampled, ensuring the preservation of any climate signal in the results. We also counted the total number of basins which crossed between tiles, which when added to the total count of all basins falling within a single tile, gives a count of the total number of drainage basins globally (Table S1).

The channel extraction method used to develop the GDBM database is designed to detect channel topography, rather than flowing rivers. At a resolution of 30 m, local roughness (topographic) differences between pixels leads to flow convergence in the flow accumulation algorithm. The accumulated flows produce channel networks from which we subsequently extract the longest channel satisfying the criteria specified above. This means that there is a reasonable likelihood of detecting and extracting a channel in an arid landscape (corresponding to the topographic gradient, Fig.S2f), in regions with significant topographic variation in the SRTM data. This aspect distinguishes GDBM from many other hydrography databases, which often remove arid channels because they are not mapped as blue lines.

The mainstem channel in each basin or subbasin exceeding the drainage area threshold, identified as the channel with the maximum flow length per basin, was then sampled on a per pixel basis to record the channel flow distance. The latitude/longitude of the most downstream point on each channel profile is stored in the database (Fig.S1a). The extracted data were then used to compute channel length (L). Drainage basin area (A) for each channel was also stored from the channel network extraction process, and it was used to compute L/A. Aridity Index values were assigned to each channel in GDBM based on the median value from every pixel along the channel profile. From these data, we compiled counts of all sampled channels by Köppen-Geiger climate zone (both subzones and major zone categories, Fig.S1b), and by Aridity Index climate categories (Fig.S1c), to create a user-friendly database that can be queried for specific data subsets. Metrics of channel relief (total drop in elevation along the channel from upstream to downstream) and channel gradient (mean slope along the topographic channel profile) are also included in the GDBM database, although they are not discussed here.

Aridity Index values were sampled at the centroid of every channel pixel, yielding an average sampling frequency of 36 meters along the length of each channel. From these sampled values, the mean and median Aridity Index values were computed, along with the standard deviation and the maximum and minimum values of Aridity Index. The number of samples recorded for a channel is also reported, to allow users of GDBM to only select basins for further study that have an adequate number of measurements. Individual channels with a small number of Aridity Index measurements along their length (< 10) occur in GDBM due to the discrepancy between the resolution of the SRTM dataset (~30 m) and the Aridity Index dataset (~900 m). However, they are rare, accounting for 23 channels, or 0.01% of GDBM.

Our analysis was performed on the latest SRTM dataset (Shuttle Radar Topography Mission (SRTM) - NSF OpenTopography Facility-doi:10.5069/g9445jdf, 2013), which has an approximate spatial resolution of 30 meters, which allows smaller channels to be identified, and more detail to be resolved within extracted channels, increasing the utility of these data beyond the goals of this paper. The structure of GDBM as a relational database of drainage basin topographic metrics also facilitates much more rapid analysis of global scale basin geometry and climate signatures than previous datasets, which have a focus predominantly on the location of channels and provision of these data in GIS formats. In all, GDBM includes ~9 million km of channel length, equivalent to ~225 times the Earth's circumference, within 115 million km^2 of global land area (Table S1).

We checked whether our channel length results (e.g., Fig.1) might be affected by sinuosity and further, whether our extraction method captures channel sinuosity for the 30-m SRTM data. We tested that GDBM is adequately capturing the true lateral geometry of channels by measuring reach-scale sinuosity across the entire dataset. Each channel in the dataset was broken into approximately 10-km long reaches and sinuosity was calculated as the ratio of the along-channel distance divided by the Euclidean distance between the start and end of that reach. If this sinuosity ratio is greater than 1, the flow length of a reach is longer than the Euclidean distance, indicating a meandering channel planform. In cases where the sinuosity ratio is equal to 1, the channel may be meandering at much longer wavelengths than 10 km, but most of our studied rivers are <100 km in length. Our tests demonstrate that our channel extraction method on 30-m SRTM data well represents channel sinuosity at a high enough fidelity to capture along-channel length (Fig.S3). In lower resolution data (e.g., 90-m SRTM), channel meanders will not be captured, resulting in artificially straight (and shorter) sections of channel. Fig.S3 shows a range

of sinuosity values from these 10-km reaches, clearly indicating that our channel extraction procedure captures channel planform meandering, so there should be no obvious bias in channel length introduced for regions with meandering channels versus those with straight channels.

GDBM Database. Our new drainage basin morphometrics database, GDBM is meant to be broadly useful to a wide range of researchers (geomorphologists, hydrologists, hydrologic modelers, land surface modelers, ecologists, biogeochemists, etc.). We provide the entire database on a long-term data storage access site. In addition to the elements described in the paper, the database also includes the latitude/longitude for the most downstream point on each channel, the country and continent in which the most downstream point resides, the relief and slope of each extracted channel, and statistics on downstream variations in Aridity Index along the channel.

Analysis of GDBM. We analyzed the metrics contained within GDBM in several ways. First, we organized data by Köppen-Geiger main climate zones and subzones (Fig.1a,c;Figs.S4;S5), as well as by major Aridity Index climate categories (Fig.1b,d). For each of these categories, we computed the total number of basins contained within each, the total length of channel (L) for basins entirely contained within a single climate zone, drainage basin area (A), and L/A (Table S1).

We used the GDBM data to generate violin plots in Matlab (https://github.com/bastibe/Violinplot-Matlab). These plots are enhancements of standard boxplots because they use kernel density estimation to generate box widths that represent the density of values at each magnitude. This is how we generated the plots in Figs.S3-S5. To generate Fig.2 and Figs.S6 and S7, we used the *binscatter* function within Matlab. We computed Hack's Law exponents based on a fixed value of the coefficient based on the fit for all data (0.554). In other words, we fixed the y-intercept and evaluating the slope on the relationship between L and A. To further explore how the coefficient in Hack's Law might vary with climate, we separately fixed h based on the fit for all data (0.758) and allowed c to vary. This analysis (not included in Fig 2) showed that c also increases monotonically with aridity as follows: 0.516 (Humid), 0.522 (Dry Subhumid), 0.546 (Semi-arid), 0.610 (Arid), 0.690 (Hyperarid). We include this here since it has been suggested that c in Hack's Law specifically represents basin shape, such that higher values indicate more elongate basins (Sassolas-Serrayet et al., 2018). This result is consistent with our interpretation of downstream channel extension and preservation in increasingly arid environments.

To evaluate our computed metrics and compare them, we checked whether the compiled GDBM metrics for each climate zone (category) are statistically distinct from one another, using the two-sample Kolmogorov-Smirnov test in a pairwise manner (using Matlab's function *kstest2*). Statistics and p-values for these comparisons are contained within Table S2 (Köppen-Geiger climate zones and Aridity Index climate categories). In Matlab there is a minimum p-value of 1.00E-323, thus the preponderance of such values in these tables. It must be noted that tests of statistical difference between distributions are often affected by large sample sizes, such that all K-S tests performed here yielded significant differences between Köppen-Geiger and Aridity Index climate classes. However, large differences between climate zones and categories are easily identified by very low p-values. For example, channel length comparisons between Arid and other climate zones for the Köppen-Geiger zones yielded p-values at the minimum value (1.00E-323). This p-value can be easily contrasted with, for example, the p-value of 3.54E-21 for the comparison of channel length between Temperate and Tropical zones (Table S2). In other words, the distributions of length values within Temperate and Tropical zones are much more similar to one another than those for Arid and any other zone, in spite of the statistical difference between Temperate and Tropical zones. We also used the Kruskal-Wallis (K-W) test (a non-parametric version of ANOVA) to compare distribution medians between climate categories in both classification schemes (Table S3). Again, due to large sample size, many of these tests yielded significant differences, so we thresholded the dataset at 1.00E-5 to identify highly significant differences between distribution medians. To better identify the most significant differences between distributions for all climate categories, we highlighted in Tables S2 and S3 with grey shading p-values less than 1.00E-50 for K-S and 1.00E-5 for K-W.

Hack's Law. Our analysis of Hack's Law was based on using a single data pair of *L* and *A* for each basin or subbasin that exceeded our area threshold. This sits in contrast to the original work by Hack and others that followed, which plotted multiple data pairs with increasing distance downstream along the stream channel. In our analysis of GDBM, we found ~2 orders of magnitude of scatter in the Hack power law relationship (Fig.2), which indicates Hack's Law may be more limited than previously thought. One reason for the strong difference in scatter between our analysis and that of Hack may be a function of statistical independence. Specifically, each of our data points was generated from an individual channel, thus satisfying the assumption of independent and identically distributed random variables (IID), while Hack's original plot includes data from multiple locations on each stream. Therefore, Hack's data are not IID, due to serial correlation (each length-area point is inherently related to the other points on the same channel). This may explain the lower amount of scatter in Hack's original plot (Hack, 1957).

We also found a large difference between the global average Hack's *h* from GDBM (0.758) compared to what has been previously reported (~0.6) (Hack, 1957). We believe this difference is merely a consequence of two different methods for quantifying channel length. Our method uses along-channel length, while many prior efforts simply used channel axis as a Euclidean distance. This is supported by previous work showing that strong differences in Hack's *h* can be obtained by using different methods of computing channel length (Willemin, 2000). For example, Table 1 in (Willemin, 2000) showed that *h* for the same river in Oregon varied from 0.7 for along-channel length (our method) to 0.52 when using Euclidean distance. This illustrates that accounting for along-channel distance, incorporating sinuosity (Fig.S3a) in length calculations may reasonably lead to overall higher values of Hack's exponent. To test this further, we selected a random sample of ~10,000 channels from GDBM, and we plotted Euclidean distance from the start to the end point of each channel against basin area. We plotted these data and calculated *h* for comparison with *h* computed via the along-channel method. We found that the Euclidean distance method resulted in an *h* value of 0.58, which is more in line with previous literature, while the along-channel distance method produced an *h* value of 0.78 (Fig.S3b-c). We believe our method is a more accurate characterization of channel length, and owing to the large sample size in GDBM, our global average of Hack's *h* is thus a more robust estimate than presented in previous work.

In addition to the climate dependence on Aridity Index discussed in the paper, we also show that Hack's *h* varies for Köppen-Geiger zones. In particular, we found that *h* is highest for the Arid Köppen-Geiger zone and lowest for the Cold zone (Fig.S6). Previous work has suggested there may be an area dependence within Hack's law, so we classified the GDBM data by area bins and recomputed Hack's *h* for each bin. The results show that Hack's Law is not scale dependent for the relatively small basin areas contained within GDBM (Fig.S7). The scale dependence in *h* that has been documented elsewhere (Rigon et al., 1996) only occurs at drainage areas >20,000 km^2. Basins of this scale were generally excluded from GDBM, since they more likely cross Köppen-Geiger climate subzones.

Timescales of Basin Evolution. In our paper, we do not explicitly address the timescale over which climate creates an imprint within drainage basins. We instead show that we can detect relationships between topographic metrics from basins and climate classifications. Clearly, the time required to evolve the landscape is dependent on the expression of its climate regime, which differs for different regions. Arid regions have less frequent rainfall and flooding, so it

might take longer for the climate signal to be expressed in these regions, compared to humid regions, which have a more regular climate expression. Here we work under the assumption that the current climate regime (that which is reflected in either Köppen-Geiger or Aridity Index climate classifications) has prevailed for long enough in each drainage basin such that the morphometrics reflect the drainage basin evolution under this climate. Clearly, there may be cases in which climate change has dramatically altered the processes and patterns of drainage basin development, but we see these as the exception, rather than the rule. We assume, for example, that arid regions have been arid for long enough to record the climate signature of aridity within their drainage basins, even if they preserve signatures of ancient flood events (Rinaldo et al., 1995). Furthermore, when looking at drainage basin morphometrics from any channel (even on Mars or other solar system bodies), we can only speculate about the forces that shaped the channel network, but we can be confident that larger flood events will be better preserved in topography than smaller ones (Singer & Michaelides, 2014; Wolman & Gerson, 1978).

GDBM v. GLoPro. We previously published a study showing how river longitudinal profiles segregate by aridity, in which we showed that straight profiles are more common in dry climate regions(Chen et al., 2019). That paper showed that aridity is also a dominant control on longitudinal profile concavity through its expression in stream hydrology. The previous study generated a dataset of Global Longitudinal Profiles (GLoPro), which includes the topographic profiles along each channel (elevation versus distance), the latitude/longitude of the most downstream point on each channel, the classification of each channel based on Köppen-Geiger and Aridity Index classification systems, and the normalized concavity index (NCI). The GDBM dataset presented here is largely based on the same channel locations (same reported downstream point on each channel), but the dataset is otherwise distinct. The GDBM dataset has fewer basins/channels overall than GLoPro, since here we adopted a uniform threshold drainage area threshold that does not vary by latitude. The GDBM dataset includes the following information for each channel: length, drainage basin area, *L/A*, total channel relief, and average channel gradient. We view GDBM and GLoPro as complementary datasets. However, the results presented here should be considered independent of those in the previous work. Namely, the arid channels that exhibited straight profiles within GLoPro should not be considered the same as those which are longer with larger basin areas with GDBM. In both databases, there is considerable overlap between climate classifications that arises due to a range of factors that we did not control for. Furthermore, we view these sets of climate signatures as independent of each other, based on the controlling processes and the timescales over which they occur.

Specifically, relatively straight long profiles in drylands evolve based on the time integral of all flows in the channel that are capable of eroding the channel bed and shaping the profile, in which a similar flow integral of flow-based erosion occurs everywhere along the channel (Chen et al., 2019). In contrast, aridity expresses within channel length, *L/A*, and Hack's *h* due to the topographic preservation of brief episodic flood events that extend the channel downstream. Thus, the results presented here likely occur based on the frequency of extreme high-flow events, rather than the integral of all events above a threshold. Thus, it is not surprising that long channels with large drainage basins do not necessarily have straight longitudinal profiles.

Supplementary Figures

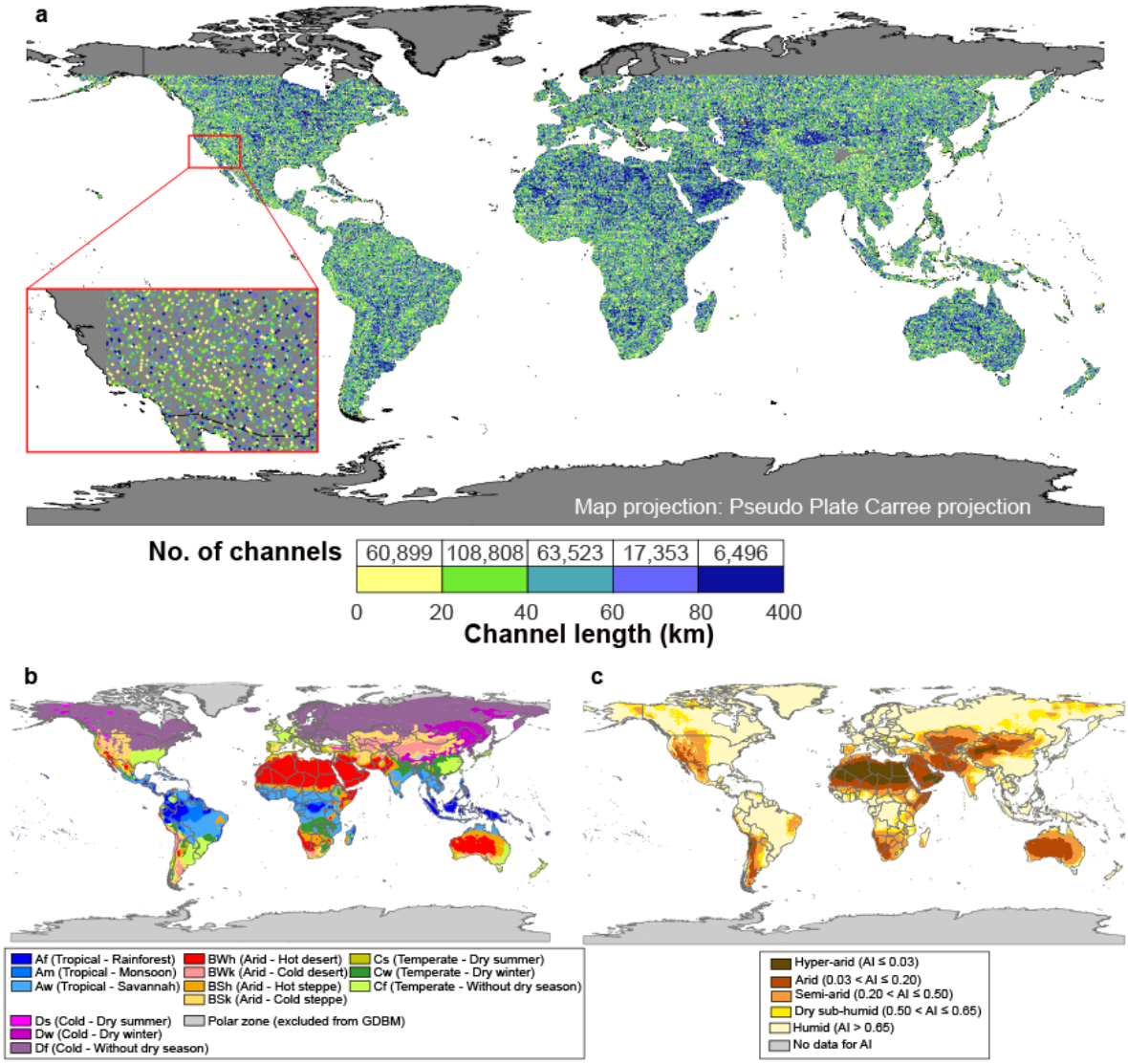

Fig.S1 | Maps of analyzed channels in climate context. **a,** Map showing most downstream point on each channel included in GDBM, color coded by bins of channel length. **b,** Global map of Köppen-Geiger climate classification from (Peel et al., 2007). **c,** Global map of Aridity Index (data source of the background map: Natural Earth (https://www.naturalearthdata.com/). Note: the data are only available between 60°N and 56°S, corresponding to the limits of the SRTM 30-m dataset.

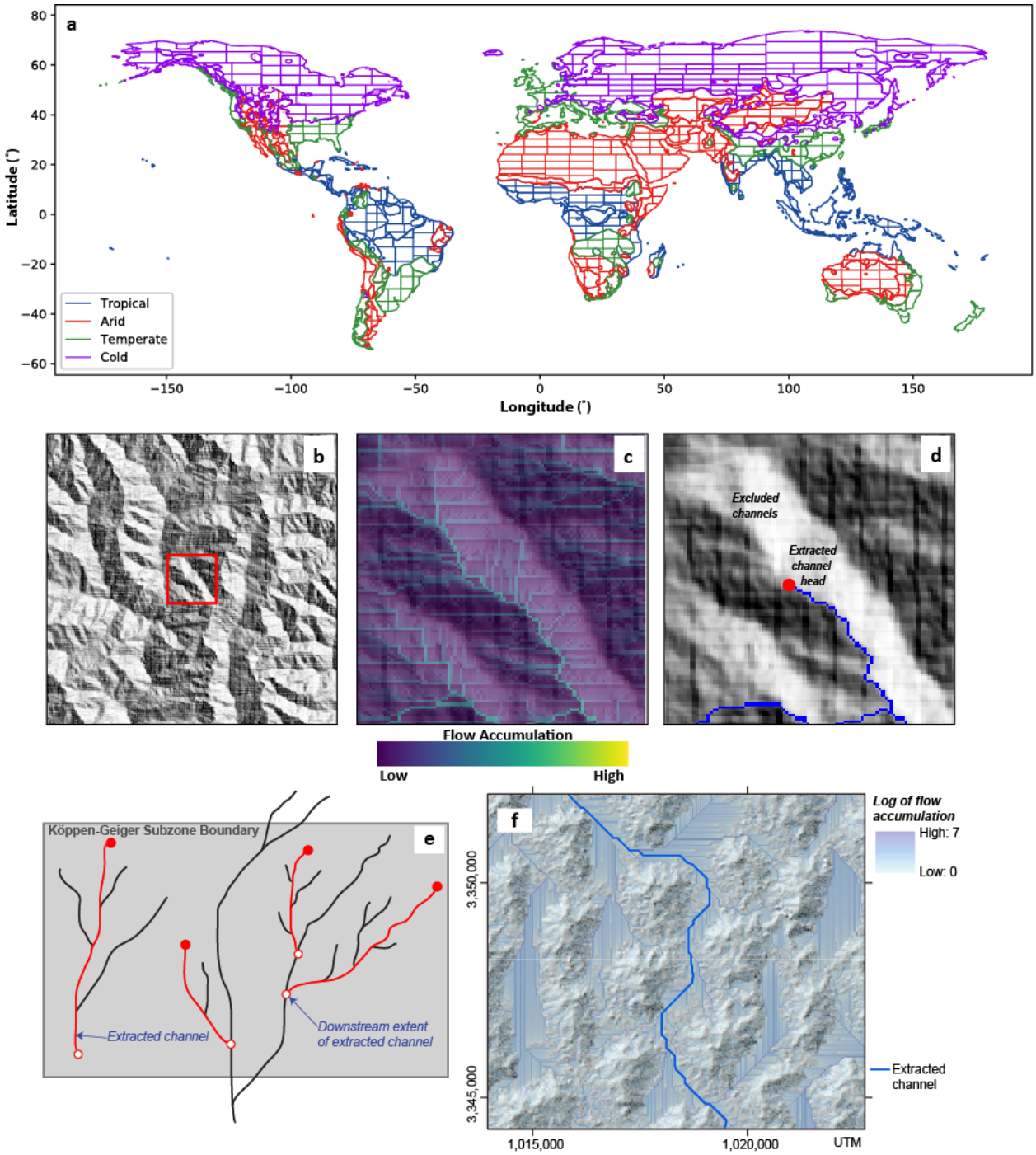

Fig.S2 | Schematic outlining channel extraction methodology. **a,** Map showing tiles used to extract channels across the globe. **b,** Shaded relief of a 70.5 km^2 area of Northern California. Red box shows location of **c** and **d**. **c,** Logarithmically scaled flow accumulation map, showing concentration of flow in valley bottoms, higher values correspond to a higher likelihood of a channel being present. **d,** Channel head (red circle) and channel (blue) flowing downslope from channel head, following the line of steepest descent. The area covered in **c** and **d** is 7.8 km^2. The area threshold for a channel in GDBM is ~22.5 km^2, so channels with smaller upstream areas were excluded from GDBM. **e,** Schematic of the selection of extraction channels for inclusion in GDBM. The method requires that the extracted channel is the longest in its basin or subbasin, but which does not cross Köppen-Geiger subzone boundaries. Channel length is measured as distance from

channel head (solid red circle) to most downstream point (white circle with red boundary). Multiple channels (subbasins) may be included, as long as they satisfy the drainage area threshold and do not cross Köppen-Geiger subzone boundaries. **f,** Dominant channel extraction in the drylands of the Grand Erg Oriental (Sahara Desert) based on the flow accumulation algorithm in LSDTopoTools. The image shows that although there are many parallel drainages derived from D8 flow accumulation, these channels ultimately converge, so that only a single dominant channel is included in the database according to the criteria listed above. Note: the extracted channel does not appear as a blue line on topographic maps, so it would not be included in hydrography databases or hydrography/DEM products that use drainage enforcement.

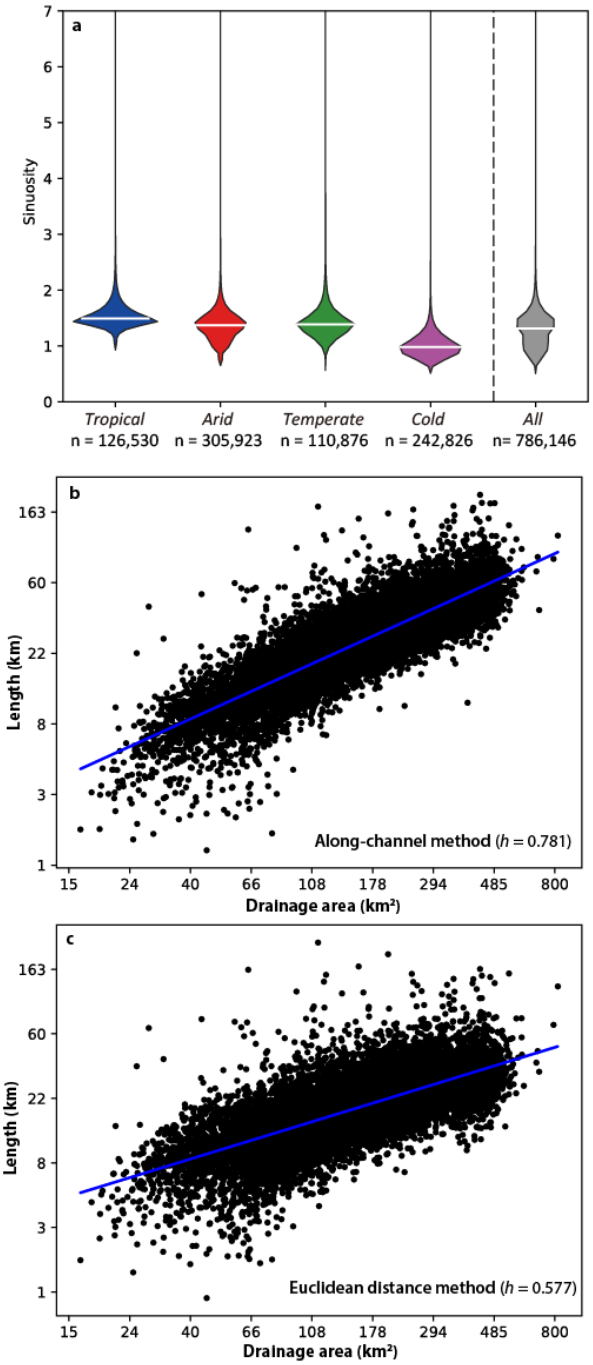

Fig.S3 | Sinuosity and its impact on Hack's h. **a,** Reach-scale sinuosity for the four main climate zones (Köppen-Geiger), and the full dataset. Values below labels indicate the number of 10-km reaches sampled for a given category. White bar on each violin plot denotes the median value. **b,** Hack's Law relationship for along-channel distance method (accounting for sinuosity). **c,** Hack's Law relationship for Euclidean distance method.

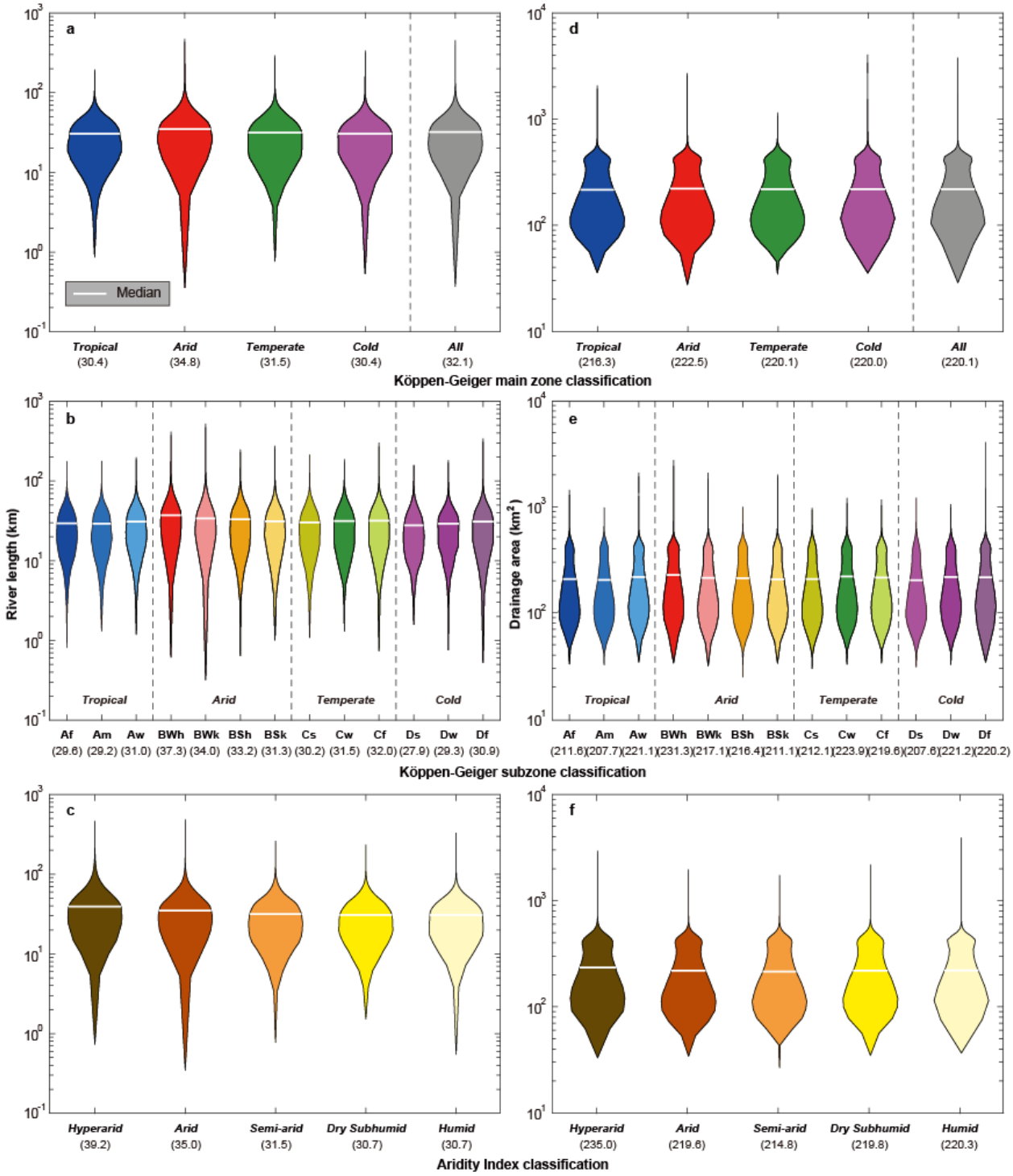

Fig.S4 | Drainage basin metrics from GDBM classified by climate. We show detailed sub-categories of Köppen-Geiger and all available data for length (**a-c**) and drainage basin area (**d-f**) for Köppen-Geiger main climate zones (**a,d**), Köppen-Geiger climate subzones (**b,e**), and Aridity Index classes (**c,f**). Plots are based on channels contained entirely within a single Köppen-Geiger subzone. Colors correspond to Köppen-Geiger subzones and Aridity Index classes (Fig.S1b,c). Median values for each sub-category are listed below each plot.

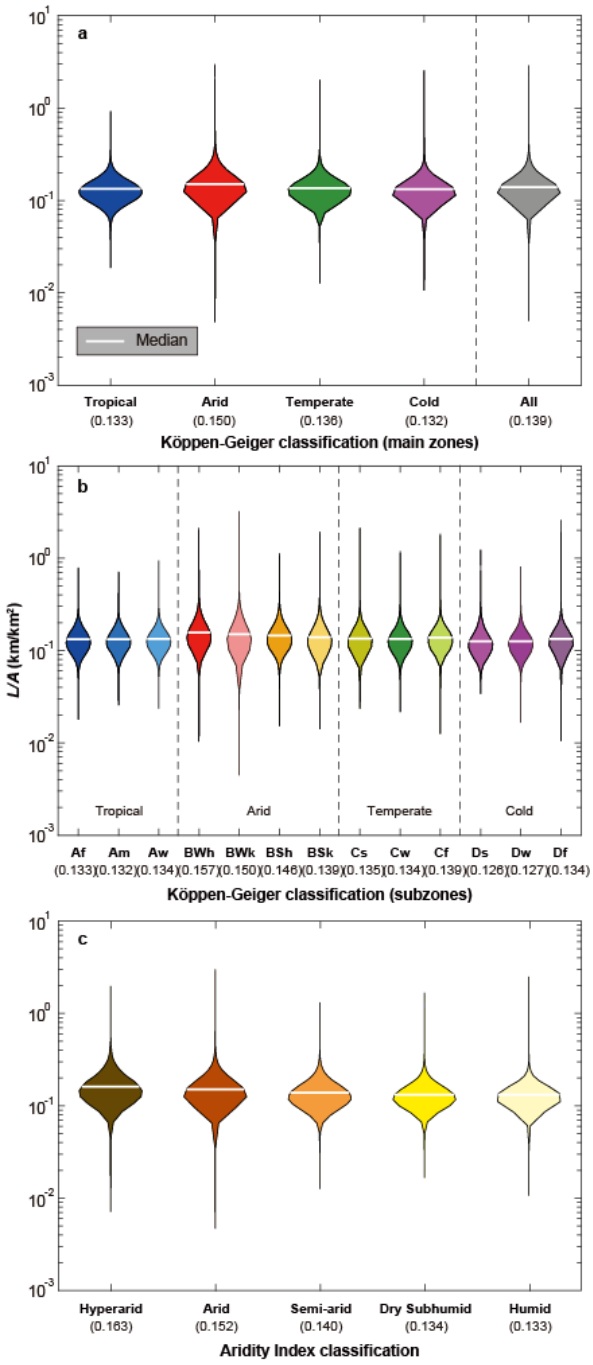

Fig.S5 | *L/A* from GDBM classified by climate. We show detailed sub-categories of Köppen-Geiger and all available data for *L/A* for Köppen-Geiger main climate zones (**a**), Köppen-Geiger climate subzones (**b**), and Aridity Index classes (**c**). Colors correspond to Köppen-Geiger subzones and Aridity Index classes (Fig.S1b,c). Median values for each sub-category are listed below each plot.

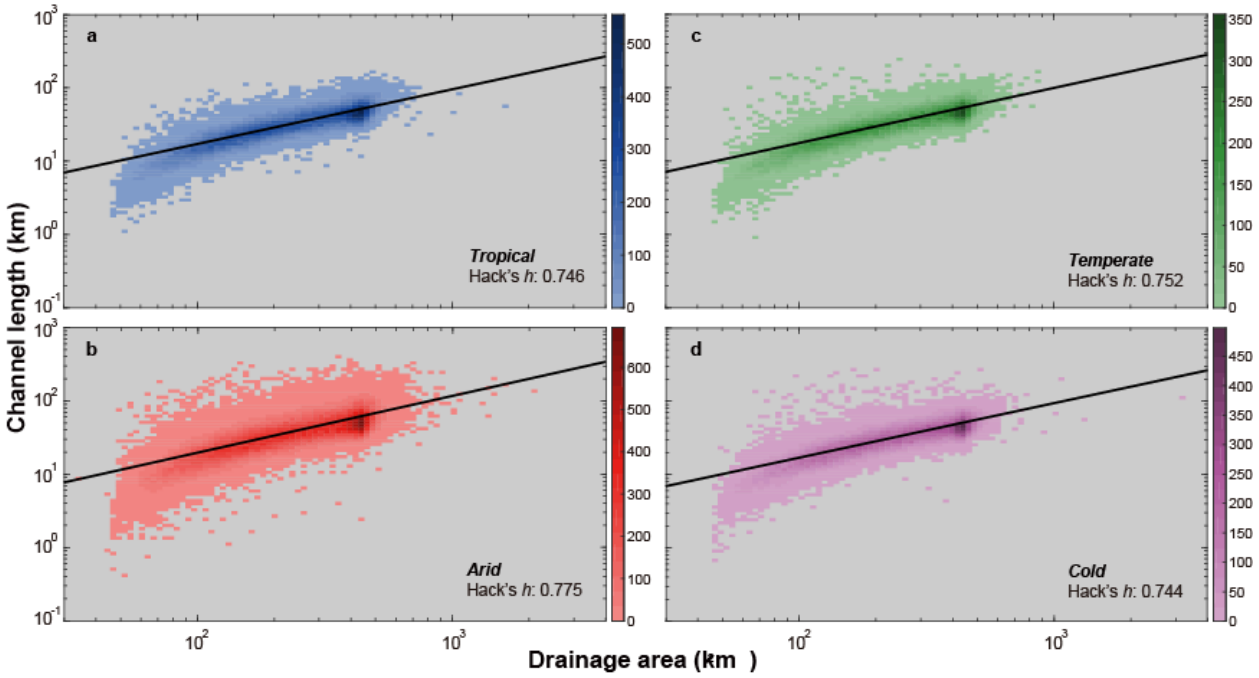

749

750 **Fig.S6 |** Climate-classified Hack's Law. Data by Köppen-Geiger category for relationships between
751 channel length (*L*) and drainage area (*A*). Density of points in areas of the scatterplot are shown
752 in the scale bars to the right of each panel. The Hack exponents for each panel (**a-d**) indicate a
753 climatic dependency on the steepness of this relationship, where arid basins exhibit the highest
754 value of *h*.

755

756

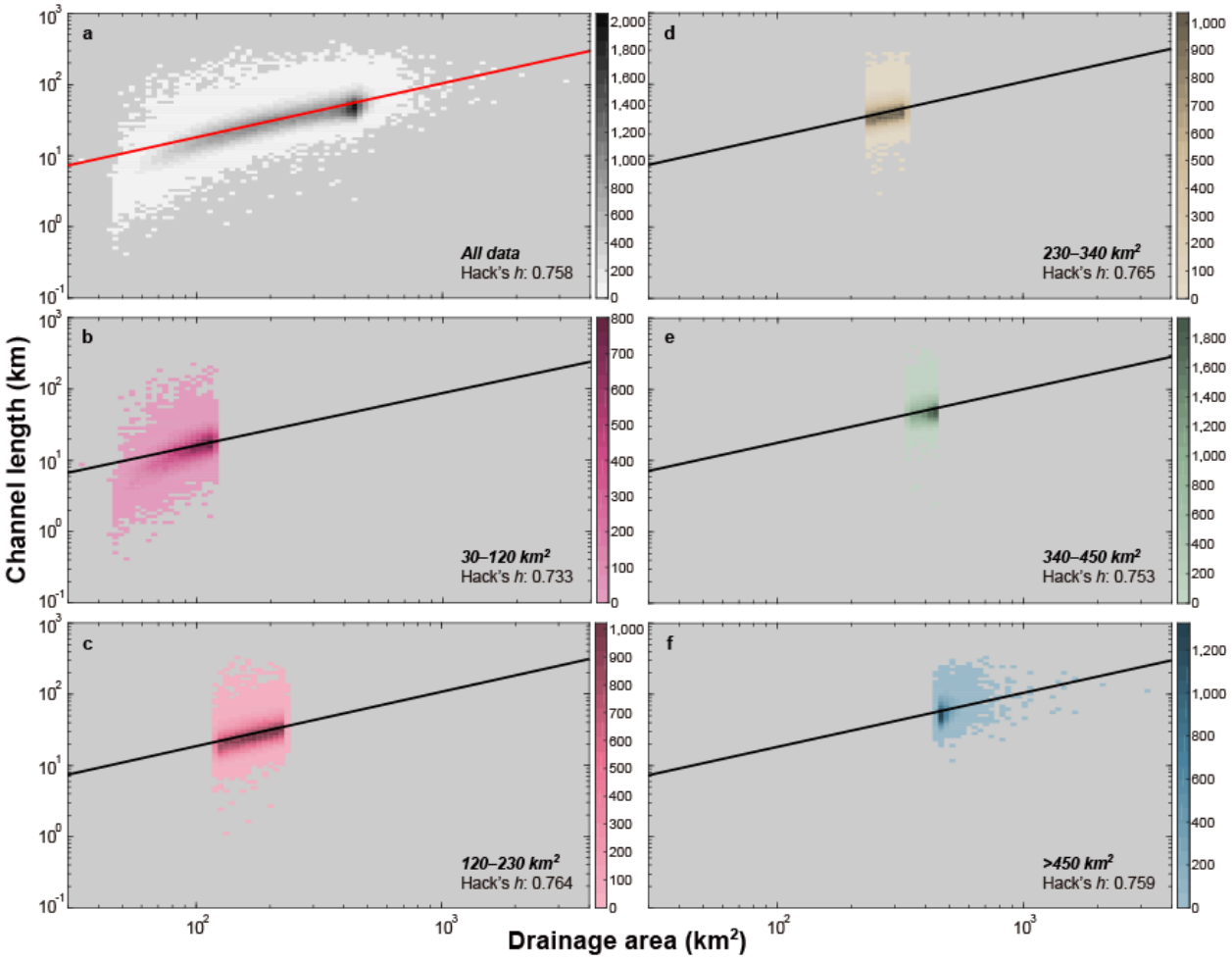

Fig.S7 | Hack's Law power fits for different bins of drainage basin area. Density of points in areas of the scatterplot are shown in the scale bars to the right of each panel. Panel **a** contains all the data and panels **b-f** contain data for different area bins. There is no significant variation in Hack's *h* by area for the range of basin sizes contained within GDBM.

Supplementary Tables

Table S1 | Summary data on number of drainage basins, area, total length by Köppen-Geiger climate zones (**a**) and Aridity Index categories (**b**). Colors correspond to maps in Fig.S1b,c.

a) RELEVANT K-G DATA

Climate sub-zone	Af	Am	Aw	BWh	BWk	BSh	BSk	Cs	Cw	Cf	Ds	Dw	Df	
No. of channels	14,114	10,581	37,084	46,999	13,040	18,408	18,827	5,785	15,794	20,972	2,318	12,169	40,988	
Climate main zone			Tropical				Arid			Temperate			Cold	Main zones total
No. of channels			61,779				97,274			42,551			55,475	257,079
Multiple zones	Af	Am	Aw	BWh	BWk	BSh	BSk	Cs	Cw	Cf	Ds	Dw	Df	Multiple zones total
No. of channels	6059	5666	12072	11515	4913	6948	9276	3818	4521	14069	1597	3147	14443	98,044
Climate sub-zone	Af	Am	Aw	BWh	BWk	BSh	BSk	Cs	Cw	Cf	Ds	Dw	Df	
Clipped Area (km^2)	6,144,065	5,009,227	17,145,309	20,010,965	6,936,283	7,952,759	10,079,873	3,024,883	6,834,180	10,098,897	923,080	4,438,341	16,391,045	
Climate main zone			Tropical				Arid			Temperate			Cold	Main zones total
Clipped Area (km^2)			28,298,600				44,979,880			19,957,960			21,752,465	114,988,905
Climate sub-zone	Af	Am	Aw	BWh	BWk	BSh	BSk	Cs	Cw	Cf	Ds	Dw	Df	
Total Length (km)	446,998	327,969	1,221,818	1,953,189	502,366	661,593	639,604	186,930	531,130	716,606	69,829	374,218	1,352,258	
Climate main zone			Tropical				Arid			Temperate			Cold	Main zones total
Total Length (km)			1,996,785				3,756,753			1,434,666			1,796,305	8,984,508

Multiple zones	Grand Total
	355,123

b) RELEVANT AI DATA

AI Climate Category	Hyperarid	Arid	Semi-arid	Dry Subhumid	Humid	All
No. of channels	19,145	48,033	51,453	24,236	114,201	257,068
Clipped Area (km^2)	5,741,619	14,735,228	18,202,791	11,850,357	64,458,911	114,988,905
Total Length (km)	851,989	1,852,702	1,754,338	800,389	3,724,981	8,984,399

Table S2 | Kolmogorov-Smirnov statistics for comparisons between Köppen-Geiger climate zones (**a**) and Aridity Index climate categories (**b**) for channel length, drainage area, and *L/A*. Grey shading indicates highly significant differences between distributions (p-values less than 1.00E-50).

a) K-G KOLMOGOROV-SMIRNOV STATISTICS		*L*		*A*		*L/A*	
K-G climate main zone comparison		p-value	K-S Statistic	p-value	K-S Statistic	p-value	K-S Statistic
Tropical	Arid	1.00E-323	1.09E-01	3.69E-07	1.43E-02	1.00E-323	1.72E-01
Tropical	Temperate	3.54E-21	3.08E-02	1.24E-02	1.00E-02	7.67E-24	3.27E-02
Tropical	Cold	7.22E-02	7.50E-03	2.17E-02	8.80E-03	3.73E-13	2.24E-02
Arid	Temperate	8.83E-163	7.94E-02	8.74E-02	7.30E-03	1.00E-323	1.44E-01
Arid	Cold	1.00E-323	1.14E-01	9.19E-02	6.60E-03	1.00E-323	1.73E-01
Temperate	Cold	4.89E-27	3.56E-02	5.59E-01	5.10E-03	1.03E-39	4.33E-02

b) AI KOLMOGOROV-SMIRNOV STATISTICS		*L*		*A*		*L/A*	
Aridity Index category comparison		p-value	K-S Statistic	p-value	K-S Statistic	p-value	K-S Statistic
Hyperarid	Arid	1.16E-89	8.65E-02	6.86E-16	3.60E-02	5.83E-79	8.12E-02
Hyperarid	Semi-arid	1.00E-323	1.64E-01	5.28E-27	4.68E-02	1.00E-323	1.88E-01
Hyperarid	Dry Subhumid	1.93E-318	1.85E-01	1.04E-11	3.48E-02	1.00E-323	2.52E-01
Hyperarid	Humid	1.00E-323	1.92E-01	2.91E-17	3.44E-02	1.00E-323	2.68E-01
Arid	Semi-arid	1.33E-132	7.82E-02	1.20E-03	1.22E-02	2.25E-254	1.08E-01
Arid	Dry Subhumid	6.55E-142	1.01E-01	3.34E-01	7.40E-03	1.00E-323	1.74E-01
Arid	Humid	1.00E-323	1.06E-01	9.68E-02	6.70E-03	1.00E-323	1.89E-01
Semi-arid	Dry Subhumid	3.67E-09	2.47E-02	5.15E-04	1.58E-02	5.86E-64	6.66E-02
Semi-arid	Humid	7.45E-27	2.93E-02	5.35E-07	1.46E-02	9.23E-208	8.20E-02
Dry Subhumid	Humid	1.17E-02	1.13E-02	7.32E-01	4.90E-03	3.49E-06	1.82E-02

Table S3 | Kruskal-Wallis statistics for comparisons between Köppen-Geiger climate zones (**a**) and Aridity Index climate categories (**b**) for channel length, drainage area, and *L/A*. Grey shading indicates highly significant differences between distributions medians (p-values less than 1.00E-5).

a) K-G KRUSKAL-WALLIS STATISTICS		*L*		*A*		*L/A*	
K-G climate main zone comparison		p-value	K-W Statistic	p-value	K-W Statistic	p-value	K-W Statistic
Tropical	Arid	3.77E-09	-1.84E+04	1.72E-05	-1.79E+03	3.77E-09	-2.72E+04
Tropical	Temperate	3.77E-09	-4.79E+03	1.19E-02	-1.43E+03	3.77E-09	-5.10E+03
Tropical	Cold	1.00E+00	2.73E+01	5.13E-02	-1.11E+03	9.04E-07	2.28E+03
Arid	Temperate	3.77E-09	1.36E+04	8.43E-01	3.55E+02	3.77E-09	2.21E+04
Arid	Cold	3.77E-09	1.84E+04	3.18E-01	6.75E+02	3.77E-09	2.94E+04
Temperate	Cold	3.77E-09	4.82E+03	9.09E-01	3.20E+02	3.77E-09	7.38E+03

b) AI KRUSKAL-WALLIS STATISTICS		*L*		*A*		*L/A*	
Aridity Index category comparison		p-value	K-W Statistic	p-value	K-W Statistic	p-value	K-W Statistic
Hyperarid	Arid	9.92E-09	1.42E+04	9.92E-09	6.11E+03	9.92E-09	1.52E+04
Hyperarid	Semi-arid	9.92E-09	2.75E+04	9.92E-09	7.90E+03	9.92E-09	3.28E+04
Hyperarid	Dry Subhumid	9.92E-09	3.07E+04	9.93E-09	5.17E+03	9.92E-09	4.32E+04
Hyperarid	Humid	9.92E-09	3.18E+04	9.92E-09	5.30E+03	9.92E-09	4.50E+04
Arid	Semi-arid	9.92E-09	1.33E+04	1.39E-03	1.79E+03	9.92E-09	1.76E+04
Arid	Dry Subhumid	9.92E-09	1.65E+04	4.86E-01	-9.46E+02	9.92E-09	2.80E+04
Arid	Humid	9.92E-09	1.76E+04	2.54E-01	-8.17E+02	9.92E-09	2.98E+04
Semi-arid	Dry Subhumid	2.19E-07	3.24E+03	2.26E-05	-2.73E+03	9.92E-09	1.04E+04
Semi-arid	Humid	9.92E-09	4.30E+03	1.03E-08	-2.60E+03	9.92E-09	1.22E+04
Dry Subhumid	Humid	2.55E-01	1.06E+03	9.99E-01	1.28E+02	8.04E-03	1.74E+03

Supplementary Dataset

Dataset S1 (separate file)

The data can be downloaded in chunks by Köppen-Geiger climate subzones from this link: https://ucsb.box.com/s/92yuu1y9qadvvruoqshig963xz89hsc3. These files contain the entire database of Global Drainage Basin Morphometrics (GDBM) organized as listed above. This download link should not be shared and is only valid for the review process. Once the paper is accepted, we will post these data on a long-term data storage server.

References

Bonnet, S. (2009). Shrinking and splitting of drainage basins in orogenic landscapes from the migration of the main drainage divide. *Nature Geosci, 2*(11), 766-771. 10.1038/ngeo666. http://dx.doi.org/10.1038/ngeo666

Braun, J., & Willett, S. D. (2013). A very efficient O(n), implicit and parallel method to solve the stream power equation governing fluvial incision and landscape evolution. *Geomorphology, 180-181*, 170-179. http://www.sciencedirect.com/science/article/pii/S0169555X12004618

Carson, M. A., & Kirkby, M. J. (1972). *Hillslope Form and Process*: Cambridge University Press.

Chen, S.-A., Michaelides, K., Grieve, S. W. D., & Singer, M. B. (2019). Aridity is expressed in river topography globally. *Nature, 573*, 573–577. https://doi.org/10.1038/s41586-019-1558-8

Clubb, F. J., Mudd, S. M., Milodowski, D. T., Grieve, S. W. D., & Hurst, M. D. (2017). LSDChannelExtraction V1.0, https://doi.org/10.5281/zenodo.824198.

Collins, D. B. G., & Bras, R. L. (2008). Climatic control of sediment yield in dry lands following climate and land cover change. *Water Resources Research, 44*(10), 8. Article. <Go to ISI>://000259993200002

Collins, D. B. G., & Bras, R. L. (2010). Climatic and ecological controls of equilibrium drainage density, relief, and channel concavity in dry lands. *Water Resources Research, 46*(4), W04508. http://dx.doi.org/10.1029/2009WR008615

Dunne, T. (1990). Hydrology, mechanics, and geomorphic implications of erosion by subsurface flows. In C. G. Higgins & D. R. Coates (Eds.), *Groundwater geomorphology: The role of subsurface water in earth-surface processes and landforms* (pp. 1-28). Boulder, CO: Geol. Soc. Amer. Special Paper 252.

Grieve, S. W. D., Mudd, S. M., Milodowski, D. T., Clubb, F. J., & Furbish, D. J. (2016). How does grid-resolution modulate the topographic expression of geomorphic processes? *Earth Surf. Dynam., 4*(3), 627-653. https://www.earth-surf-dynam.net/4/627/2016/

Hack, J. T. (1957). *Studies of longitudinal stream profiles in Virginia and Maryland* (294-B). Retrieved from Menlo Park, CA:

Horton, R. E. (1945). Erosional development of streams and their drainage basins; hydrophysical approach to quantitative geomorphology. *Geol. Soc. Amer. Bull., 56*, 275-370.

Laronne, J. B., Reid, I., Yitshak, Y., & Frostick, L. E. (1994). The non-layering of gravel streambeds under ephemeral flood regimes. *Journal of Hydrology, 159*(1-4), 353-363. http://www.sciencedirect.com/science/article/B6V6C-487DTBV-16/2/208964486e0bc7aaa3836d7dad610ccb

Lehner, B., Verdin, K., & Jarvis, A. (2008). New Global Hydrography Derived From Spaceborne Elevation Data. *Eos, Transactions American Geophysical Union, 89*(10), 93-94. https://agupubs.onlinelibrary.wiley.com/doi/abs/10.1029/2008EO100001

Leopold, L., Wolman, M. G., & Miller, J. P. (1964). *Fluvial Processes in Geomorphology*. San Francisco, CA: W.H. Freeman & Co.

Leopold, L. B., & Miller, J. (1962). *Ephemeral streams: hydraulic factors and their relation to the drainage net*. Retrieved from Washington, D.C.:

Michaelides, K., Hollings, R., Singer, M. B., Nichols, M. H., & Nearing, M. A. (2018a). Spatial and temporal analysis of hillslope–channel coupling and implications for the longitudinal profile in a dryland basin. *43*(8), 1608-1621. https://onlinelibrary.wiley.com/doi/abs/10.1002/esp.4340

Michaelides, K., Hollings, R., Singer, M. B., Nichols, M. H., & Nearing, M. A. (2018b). Spatial and temporal analysis of hillslope–channel coupling and implications for the longitudinal profile in a dryland basin. *Earth Surface Processes and Landforms*. http://dx.doi.org/10.1002/esp.4340

Montgomery, D. R., & Dietrich, W. E. (1988). Where do channels begin. *Nature, 336*(6196), 232-234. <Go to ISI>://WOS:A1988Q954200042

Ouellet Dallaire, C., Lehner, B., Sayre, R., & Thieme, M. (2019). A multidisciplinary framework to derive global river reach classifications at high spatial resolution. *Environmental Research Letters, 14*(2), 024003. http://dx.doi.org/10.1088/1748-9326/aad8e9

Peel, M. C., Finlayson, B. L., & McMahon, T. A. (2007). Updated world map of the Köppen-Geiger climate classification. *Hydrol. Earth Syst. Sci., 11*(5), 1633-1644. https://www.hydrol-earth-syst-sci.net/11/1633/2007/

Perron, J. T., Kirchner, J. W., & Dietrich, W. E. (2009). Formation of evenly spaced ridges and valleys. *Nature, 460*(7254), 502-505. <Go to ISI>://WOS:000268257000036

Perron, J. T., Richardson, P. W., Ferrier, K. L., & Lapotre, M. (2012). The root of branching river networks. *Nature, 492*(7427), 100-103. 10.1038/nature11672. http://dx.doi.org/10.1038/nature11672

Rigon, R., Rodriguez-Iturbe, I., Maritan, A., Giacometti, A., Tarboton, D. G., & Rinaldo, A. (1996). On Hack's Law. *32*(11), 3367-3374. https://agupubs.onlinelibrary.wiley.com/doi/abs/10.1029/96WR02397

Rinaldo, A., Dietrich, W. E., Rigon, R., Vogel, G. K., & Rodrlguez-lturbe, I. (1995). Geomorphological signatures of varying climate. *Nature, 374*(6523), 632-635. 10.1038/374632a0. http://dx.doi.org/10.1038/374632a0

Rinaldo, A., Rodriguez-Iturbe, I., & Rigon, R. (1998). Channel networks. *Annual Review of Earth and Planetary Sciences, 26*(1), 289-327. https://www.annualreviews.org/doi/abs/10.1146/annurev.earth.26.1.289

Sassolas-Serrayet, T., Cattin, R., & Ferry, M. (2018). The shape of watersheds. *Nature Communications, 9*(1), 3791. https://doi.org/10.1038/s41467-018-06210-4

Seybold, H., Rothman, D. H., & Kirchner, J. W. (2017). Climate's watermark in the geometry of stream networks. *Geophysical Research Letters, 44*(5), 2272-2280. http://dx.doi.org/10.1002/2016GL072089

Shuttle Radar Topography Mission (SRTM) - NSF OpenTopography Facility- doi:10.5069/g9445jdf. (2013).

Singer, M. B., & Michaelides, K. (2014). How is topographic simplicity maintained in ephemeral dryland channels? *Geology, 42*(12), 1091-1094. http://geology.gsapubs.org/content/42/12/1091.abstract

Singer, M. B., & Michaelides, K. (2017). Deciphering the expression of climate change within the Lower Colorado River basin by stochastic simulation of convective rainfall. *Environmental Research Letters, 12*.

Slater, L. J., & Singer, M. B. (2013). Imprint of climate and climate change in alluvial riverbeds: Continental United States, 1950-2011. *Geology, 41*(5), 595-598. http://geology.gsapubs.org/content/41/5/595.abstract

Solyom, P. B., & Tucker, G. E. (2004). Effect of limited storm duration on landscape evolution, drainage basin geometry, and hydrograph shapes. *Journal of Geophysical Research-Earth Surface, 109*(F3). <Go to ISI>://000236711300001

Tarboton David, G., Bras Rafael, L., & Rodriguez-Iturbe, I. (1991). On the extraction of channel networks from digital elevation data. *Hydrological Processes, 5*(1), 81-100. https://doi.org/10.1002/hyp.3360050107

Tucker, G. E. (2004). Drainage basin sensitivity to tectonic and climatic forcing: Implications of a stochastic model for the role of entrainment and erosion thresholds. *Earth Surface Processes and Landforms, 29*(2), 185-205. <Go to ISI>://000189226700005

Tucker, G. E., & Bras, R. L. (2000). A stochastic approach to modeling the role of rainfall variability in drainage basin evolution. *Water Resources Research, 36*(7), 1953-1964. <Go to ISI>://000087928800028

Tucker, G. E., & Whipple, K. X. (2002). Topographic outcomes predicted by stream erosion models: Sensitivity analysis and intermodel comparison. *J. Geophys. Res., 107*(B9), 2179. http://dx.doi.org/10.1029/2001JB000162

Wang, L., & Liu, H. (2006). An efficient method for identifying and filling surface depressions in digital elevation models for hydrologic analysis and modelling. *International Journal of Geographical Information Science, 20*(2), 193-213. https://doi.org/10.1080/13658810500433453

Willemin, J. H. (2000). Hack's Law: Sinuosity, convexity, elongation. *Water Resources Research, 36*(11), 3365-3374. https://agupubs.onlinelibrary.wiley.com/doi/abs/10.1029/2000WR900229

Wolman, M. G., & Gerson, R. (1978). Relative time scales of time and effectiveness of climate in watershed geomorphology. *Earth Surface Processes & Landforms, 3*, 189-208.

Yi, R. S., Arredondo, Á., Stansifer, E., Seybold, H., & Rothman, D. H. (2018). Shapes of river networks. *Proceedings of the Royal Society A: Mathematical, Physical and Engineering Sciences, 474*(2215), 20180081.